Optical fiber hydrogen sensor using metasurfaces composed of palladium

Shunshuo Cai (蔡顺烁)[1], Wanhan Hu (胡万晗)[1], Yiman Liu (刘怡曼)[1], Juan Ning (宁 娟)[2], Sixuan Feng (冯思璇)[2], Chao Jin (晋 超)[2], Lingling Huang (黄玲玲)[1], and Xin Li (李 昕)[1*]

[1] Beijing Engineering Research Center of Mixed Reality and Advanced Display, School of Optics and Photonics, Beijing Institute of Technology, Beijing 100081, China

[2] School of Computer Science and Technology, Beijing Institute of Technology, Beijing 100081, China

*Corresponding author: lix@bit.edu.cn

Received January 5, 2022 | Accepted February 23, 2022 | Posted Online March 28, 2022

Palladium-based hydrogen sensors have been typically studied due to the dielectric function that changes with the hydrogen concentration. However, the development of a reliable, integral, and widely applicable hydrogen sensor requires a simple readout mechanism and an optimization of the fast detection of hydrogen. In this work, optical fiber hydrogen sensing platforms are developed using an optimized metasurface, which consists of a layer of palladium nanoantennas array suspended above a gold mirror layer. Since the optical properties of these palladium nanoantennas differ from the traditional palladium films, a high reflectance difference can be achieved when the sensor based on the metasurface is exposed to the hydrogen atmosphere. Finally, the optimized reflectance difference ΔR of $\sim$0.28 can be obtained when the sensor is exposed in the presence of hydrogen. It is demonstrated that this integrated system architecture with an optimized palladium-based metasurface and a simple optical fiber readout system provides a compact and light platform for hydrogen detection in various working environments.

Keywords: hydrogen detection; metasurface; palladium; optical fiber sensor.

DOI: 10.3788/COL202220.053601

1. Introduction

Hydrogen (H_2) has attracted lots of attention as a future energy source, especially due to its high energy-density, carbon-free, and pollution-free characteristics[1,2]. However, H_2 is flammable and has low ignition energy. At room temperature and pressure, H_2 exhibits a wide explosion range for concentrations (4%–75% by volume) coupled with a large flame propagation speed. Furthermore, as a colorless, odorless, extremely volatile gas, it diffuses very fast and easily, so it may eventually leak out of its container due to its small molecular size[3]. Thus, fast leaks detection equipment for all H_2-related systems is required because of such safety reasons.

Electrical H_2 gas sensors with an electrical readout employ the change in electrical conductivity upon H_2 absorption in metal. However, such electrical sensors can only show enhanced sensitivity at high working temperatures, thus raising safety issues. Alternatively, in optical sensing schemes, the change in reflectance and/or transmittance of H_2-absorbing materials is detected[4]. A fiber-based readout has arisen as well, providing numerous advantages such as safety, corrosion resistance, and suitability for remote sensing. To date, optical fiber H_2 sensors have demonstrated high performance, which propelled the technique to the hazardous areas of certain industrial environments, such as H_2 fuel filling stations or nuclear waste repository environments[5–7]. However, such optical fiber sensors have to use special architectures to interact with the outer medium. Typical optical fiber structures, including fiber gratings[8,9], tapered fibers[10], D-shape[11,12], and U-bent[13], limit large-scale production and promotion.

In contrast with other materials solving hydrogen sensitivity such as tungsten trioxide (WO_3)[14] and zinc oxide (ZnO)[15], palladium (Pd) is a particularly suitable and widely used functional material for specific H_2 detection because the reversible phase transition depends on the ambient H_2 concentrations at room temperature[16]. Hydrogenation happens due to a change in the dielectric function with the change from Pd to PdH_x. Since the H atoms occupy interstitial lattice sites (α-phase) and even saturate the Pd lattice (β-phase) at high H_2 concentrations, an increase of the lattice constant of over 10% would be achieved[17].

In recent years, two main types of Pd-based H_2 sensors are thin films and plasmonic nanoparticles[18–21]. In these two cases, the transmittance/reflectance and wavelength shift monitor can be adapted to analyze the H_2 concentration, respectively. The relative simplicity of reflectance measurements makes such Pd-material-based H_2 sensing systems more suitable for large-scale, integral sensor applications. However, Pd thin films suffer strongly from undesirable effects such as a hysteresis in the loading and unloading of H_2 and deactivation through poisoning by other gases. On the other hand, sensors based on Pd nanoparticles, which are synthesized by chemical synthesis, are limited by poor reproducibility due to the uncontrollable surface morphology of nanoparticles in chemical synthesis. Using nanoantennas is an effective alternative because of the controllable surface morphology owing to the fabrications with nanometer level accuracy, such as lithography, nanoimprinting, and others. Additionally, different nanostructure geometries and advanced optimization methods based on mathematics can be investigated to enhance the H_2 sensitivity and to calculate the suitable parameters for the complex nature of the array manufacturing to ensure the reproducibility of the sensor. Recently, H_2 detection using nanoantennas and hydrogenation of thin films have been demonstrated as well[17,22–26].

In the present work, we demonstrate an optical fiber H_2 gas sensor consisting of a commercial multi-mode optical fiber and a metasurface attached to the fiber tip. The optimized metasurface is composed of a layer of Pd nanoantennas suspended above a gold (Au) mirror layer. The reflectance of the Pd-based metasurface is ~0.6, and it shows a clear reflectance or a power change of ~0.28 or ~3.26 dB after it is exposed to H_2, indicating an excellent hydrogenation response performance. Moreover, a fiber-based reflectance readout method can be adopted to analyze H_2 concentration in our schemes. Thus, an integral remote monitoring H_2 sensing device composed of a compact optical fiber readout system and a Pd-based metasurface for harsh access H_2 detection is achieved.

2. Methods

Figure 1(a) presents the schematic of the H_2 sensing metasurface architecture. In this design, promising geometry consists of an array of Pd nanostructures, which is separated by a dielectric spacer layer from the Au film. The Au film, here, acts as a mirror, and the magnesium fluoride (MgF_2) is employed as a dielectric spacer layer. The dielectric spacer layer is used to generate a metal–insulator–metal (MIM) meta-atom, which can be treated as a Fabry–Pérot cavity to increase reflectivity[27]. Figure 1(b) shows the scheme of the H_2 sensor, which consists of a metasurface and a fiber flange plate that serves as a connector to the optical fiber. Thus, a simple optical fiber-based readout mechanism can be used, which is based on the broadband light source with a working range of 1250–1600 nm and the power meter to monitor the reflection intensity. Moreover, a polarization controller (PC) was placed upstream of the circulation to adjust and orient the state of the polarization of light so as to provide linear polarization.

Using this nanostructure layout and optical fiber-based readout mechanism, the optical reflectance R can be read out and optimized through careful tuning of the design parameters. In fact, the highest H_2 sensitivity would be achieved by maximizing the absolute reflectance difference. In this work, we thus focus on optimizing the relevant design parameters, e.g., the diameter of Pd nanodisks, the thickness of a MgF_2 spacer, to achieve a maximum ΔR. Specifically, we perform numerical calculations on a model system[28], where the Pd nanoantenna is on a MgF_2 spacer and an Au mirror, to obtain a better understanding of the optical response and the underlying physical principles and to predict an optimum sensor design.

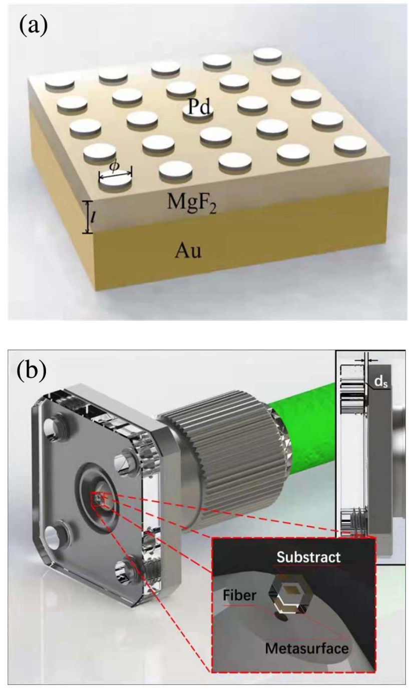

Fig. 1. (a) Schematic of the Pd-based metasurface considered in this study. Pd nanodisks are separated from an Au mirror by a dielectric spacer layer (magnesium fluoride, MgF_2). Upon H_2 absorption, the dielectric function and the size of the Pd nanodisks change, leading to a change in the reflectance spectrum of the structure. (b) The H_2 sensor is composed by a metasurface and a fiber flange plate that serves as a connector to the optical fiber. Inset: cross section of the fiber flange plate and the detail of the metasurface next to the fiber tip.

3. Results and Discussions

Numerical calculations with the finite difference time domain (FDTD) method have been carried out to gain better insight into the reflectance of the Pd nanoantennas. To investigate the behavior of the reflectance difference ΔR due to the hydrogeneration of the Pd-based metasurface, we perform simulations in Lumerical FDTD on the same system as in Fig. 1(a) with the dielectric function of the Pd disks (α-phase) and PdH disks (β-phase), where the refractive index of Pd and PdH is from the open access refractive index database[29]. Additionally, the size of the PdH disk, which we considered here in the calculation, is approximated as isotropic volume expansion of 10% compared to Pd. Because the phase transition typically occurs in Pd particles in H_2 atmosphere with a concentration of ~2% in volume[30], the Pd-based metasurface thus represents a Pd absorber structure in the presence of a H_2 concentration that is below the explosive limit (4% in volume).

Figure 2 presents a pseudocolor plot of the reflectance difference ΔR as a function of wavelength λ, the diameter of Pd disk $\varnothing_{\text{disk}}$, and thickness of the spacer layer l_{spacer}. The Pd disk thickness h_{disk} considered in the calculations is 20 nm, and the structures are periodically arranged with a period of 360 nm. As it can be seen, the reflectance difference ΔR of the Pd disk could reach ~0.3 when the diameter ranges from 150 to 250 nm, the spacer thickness ranges from 50 to 250 nm, and the wavelength range is 1200–1500 nm. Additionally, such high reflectance difference of ~0.3 can also be achieved when the Pd disk diameter is beyond 250 nm, and the wavelength range is 1500–1600 nm. Considering the period of 360 nm in this calculation, it is in fact approximated as a Pd film. Thus, such a metasurface would suffer more strongly the influence of hysteresis in the loading and unloading of H_2 due to the thermodynamics of the hybrid interaction[31,32]. Moreover, these wavelength ranges have a high loss in a multi-mode optical fiber, which we use in this case (as will be discussed below).

To explore the difference between Pd film and Pd metasurface during the progress of hydrogenation, Fig. 3 shows the reflectance of Pd (red line) as a function of varying wavelengths of incident light. Additionally, the wavelength spectrum of the reflectance of Pd hydride (black line), which considered the parameters of the β-phase, was displayed. Both of these two curves indicate that the reflectance increases with the red-shifted wavelength of incident light. The reflectance difference ΔR is also displayed in Fig. 3, and a blue curve is ΔR as a function of wavelength λ with the phase transition of Pd. The variance of the film thicknesses is ignored because there is little light passing through the metal film, and the reflectance does not change when the thickness varies. As shown in the blue curve, the

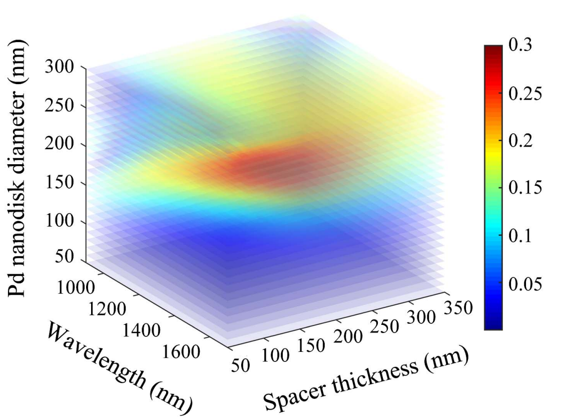

Fig. 2. Calculated reflectance difference spectra for varying Pd disk diameters and spacer thicknesses, for a disk thickness of 20 nm and period of 360 nm.

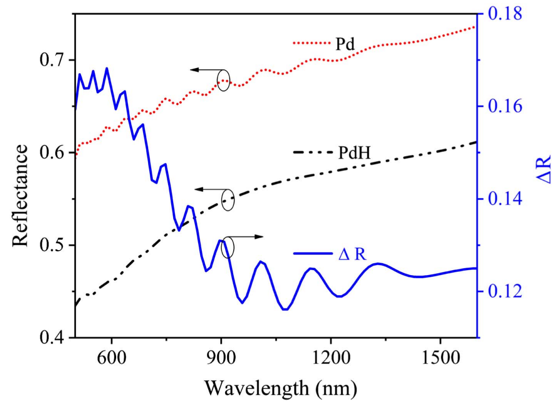

Fig. 3. Calculation of the reflectance of the Pd (red dot line) and Pd hydride (black double-dot dash line) as a function of incident wavelength.

reflectance difference is higher when the wavelength of the incident light is shorter. These results show that a higher reflectance difference ΔR can be obtained at a short wavelength of the incident light. As Fig. 3 shows, the highest reflectance difference ΔR corresponding to 0.168 can be achieved when the wavelength of the incident light is 586 nm. Compared with the results of nanoantennas, this maximum ΔR is much lower. Furthermore, unfortunately, the reflective spectrum is fixed for Pd film, and commercial communication optical fibers have a high loss at such lower wavelength. On the other hand, the working wavelength for a Pd-based metasurface can be shifted artificially to match the working wavelength of optical fibers by changing the size parameters of the nanoantenna.

Figure 4(a) presents the wavelength spectra of reflectance as a function of varying thicknesses of the spacer layer l_{spacer}. The diameter and thickness of the Pd disk are 250 nm and 20 nm, respectively. After considering the parameters of the β-phase, the counterpart's pseudocolor plot of Pd hydride can be seen in Fig. 4(b). Furthermore, reflectance difference ΔR as a function of wavelength λ and varying thicknesses of spacer l_{spacer} can be seen in Fig. 4(c).

The positions of two exemplary ΔR maxima of ~0.25 are indicated in Fig. 4(c). Both of these positions are located at the wavelength of 1200 nm and 1320 nm with the same spacer thicknesses of 150 nm. Nevertheless, these positions are not the highest or lowest reflectance of the Pd or Pd hydride, as shown in Figs. 4(a) and 4(b). A key feature of the system can find that the highest reflectance differences can be obtained via tuning the thicknesses of the spacer layer. Even though, the thickness of the spacer layer should be chosen carefully, because it could decrease the interaction as well. In particular, a response maximum very close to a region of low response cannot be chosen, since a deposition technique with high accuracy is required. The envisioned readout wavelength of the sensor, the working range of the optical fiber, should be taken into account at the same time. In this case, the reflectance difference ΔR of ~0.23 can be achieved when the spacer thickness is 150 nm and the wavelength is 1300 nm, which is located at the communication window of the common multi-mode optical fiber, as

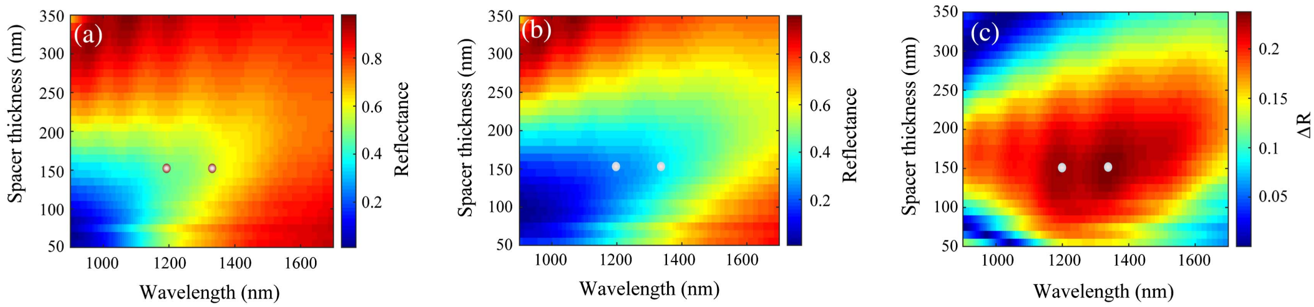

Fig. 4. Calculation of the reflectance with the varying thicknesses of the spacer layer and incident wavelength for (a) Pd disk and (b) Pd hydride disk. (c) Calculation of the reflectance difference with the varying thicknesses of the spacer layer and incident wavelength when the phase transition has happened.

shown in Fig. 4(c). Instead of the single-mode optical fiber, here, a multi-mode fiber optical fiber should be used, because the mode field distribution, which covers the area of the metasurface, is required. A multi-mode optical fiber for the working wavelength of 1300 nm (OM1, Changfei Optical Fiber and Cable Co., Ltd.) would be used.

A further simulation was performed to investigate the influence of the mode field distribution of the optical fiber. The mode field distribution was firstly calculated when the wavelength of incident light is 1300 nm using the COMSOL Multiphysics for influence evaluation. As the results show, the diameter of the mode field distribution is ∼50 μm, taking into account that the numerical aperture of the optical fiber is 0.275, and this mode field distribution could cover the whole area of the metasurface. Although the ΔR of the optimized position is not the maximum, it is the best parameter for a Pd-based metasurface for H_2 detection via a simple and economic optical fiber readout system. After that, incident light with 1300 nm and its mode field distribution is the same as the above-calculated result and was used as the incidence of a Pd-based metasurface with 61×61 array, 360 nm period, 20 nm thickness of Pd, 100 nm diameter of Pd, and 150 nm thickness of MgF_2. The calculated results show that a reflectance of the Pd-based metasurface is 0.529355, and the one after the Pd-based metasurface reacting with H_2 at 0.249729 can be achieved. In other words, a reflectance difference ΔR of ∼0.28 can be reached when the light from a multi-mode optical fiber is incident to a Pd-based metasurface. Thus, an optical fiber-based readout system would be suitable for this optimized Pd-based metasurface H_2 sensor. In addition, the reflectance difference is higher than that when the incident light was a plane wave because the wavefront from the fiber output is an inhomogeneous plane wave, and it directly impacts the result[17].

4. Conclusion

The simple optical fiber readout mechanism and an optimization of the Pd-based metasurface, which is next to the fiber tip, have been demonstrated. Suitable parameters of the metasurface, including diameter $\varnothing_{disk}$ and thickness of the Pd disk, thickness of the spacer layer l_{spacer}, and wavelength of the incident light, were calculated using the Fourier modal method. The optimized reflectance difference ΔR of ∼0.28 can be obtained when exposed to the sensor in the presence of H_2. Together with the intrinsic features of optical fibers[33], this Pd-based metasurface with an optical fiber readout system provides a promising platform for remote and harsh access H_2 detection. Moreover, the mechanism of sensor performance is a possibility to tune its spectral range of operation by the diameter and thickness of the specificity recognition materials to make this design applicable to other molecular detection applications or to positively affect the interaction between biomaterials and cells.

Acknowledgement

This work was partially supported by the National Natural Science Foundation of China (NSFC) (No. 92050117), China Postdoctoral Science Foundation (No. 2020M680370), and Beijing Institute of Technology Research Fund Program for Young Scholars (No. XSQD-201904005).

References

1. X. She, Y. Shen, J. Wang, and C. Jin, "Pd films on soft substrates: a visual, high-contrast and low-cost optical hydrogen sensor," Light Sci. Appl. **8**, 4 (2019).
2. M. Xiao, S. Liang, J. Han, D. Zhong, J. Liu, Z. Zhang, and L. Peng, "Batch fabrication of ultrasensitive carbon nanotube hydrogen sensors with sub-ppm detection limit," ACS sensors **3**, 749 (2018).
3. S. Pascuzzi, I. Blanco, A. S. Anifantis, and G. Scarascia-Mugnozza, "Hazards assessment and technical actions due to the production of pressured hydrogen within a pilot photovoltaic-electrolyser-fuel cell power system for agricultural equipment," J. Agr. Eng. **47**, 88 (2016).
4. S. A. Chowdhury, R. Correia, D. Francis, S. J. Brooks, B. J. Jones, A. W. Thompson, J. Hodgkinson, and R. P. Tatam, "An optical fiber hydrogen sensor using a palladium-coated ball lens," J. Lightwave Tech. **33**, 2535 (2015).
5. F. A. A. Nugroho, I. Darmadi, L. Cusinato, A. Susarrey-Arce, H. Schreuders, L. J. Bannenberg, A. B. da Silva Fanta, S. Kadkhodazadeh, J. B. Wagner, T. J. Antosiewicz, A. Hellman, V. P. Zhdanov, B. Dam, and C. Langhammer, "Metal–polymer hybrid nanomaterials for plasmonic ultrafast hydrogen detection," Nat. Mater. **18**, 489 (2019).
6. A. Baldi, T. C. Narayan, A. L. Koh, and J. A. Dionne, "*In situ* detection of hydrogen-induced phase transitions in individual palladium nanocrystals," Nat. Mater. **13**, 1143 (2014).

7. M. Aleixandre, P. Corredera, M. L. Hernanz, and J. Gutierrez-Monreal, "Development of fiber optic hydrogen sensors for testing nuclear waste repositories," Sens. Actuat. B Chem. **107**, 113 (2005).
8. H. Guo, J. Tang, X. Li, Y. Zheng, H. Yu, and H. Yu, "On-line writing identical and weak fiber Bragg grating arrays," Chin. Opt. Lett. **11**, 030602 (2013).
9. J. Dai, L. Zhu, G. Wang, F. Xiang, Y. Qin, M. Wang, and M. Yang, "Optical fiber grating hydrogen sensors: a review," Sensors **17**, 577 (2017).
10. X. Zhang, J. Xiong, F. Gu, J. Li, W. Wang, F. Pang, and T. Wang, "Fabrication and sensing characteristics of intrinsic Fabry–Perot interferometers in fiber tapers," Chin. Opt. Lett. **13**, 120602 (2015).
11. Z. L. Poole, P. R. Ohodnicki, A. Yan, Y. Lin, and K. P. Chen, "Potential to detect hydrogen concentration gradients with palladium infused mesoporous-titania on D-shaped optical fiber," ACS sensors **2**, 87 (2017).
12. J. Dai, M. Yang, Y. Chen, K. Cao, H. Liao, and P. Zhang, "Side-polished fiber Bragg grating hydrogen sensor with WO_3-Pd composite film as sensing materials," Opt. Express **19**, 6141 (2011).
13. M. Divagar, A. Gowri, S. John, and V. V. R. Sai, "Graphene oxide coated U-bent plastic optical fiber based chemical sensor for organic solvents," Sens. Actuat. B Chem. **262**, 1006 (2018).
14. E. Navarrete, C. Bittencourt, P. Umek, D. Cossement, F. Güell, and E. Llobet, "Tungsten trioxide nanowires decorated with iridium oxide nanoparticles as gas sensing material," J. Alloy. Com. **812**, 152156 (2020).
15. K. Anand, O. Singh, M. P. Singh, J. Kaur, and R. C. Singh, "Hydrogen sensor based on graphene/ZnO nanocomposite," Sens. Actuat. B Chem. **195**, 409 (2014).
16. C. Wadell, S. Syrenova, and C. Langhammer, "Plasmonic hydrogen sensing with nanostructured metal hydrides," ACS Nano **8**, 11925 (2014).
17. F. Sterl, N. Strohfeldt, S. Both, E. Herkert, T. Weiss, and H. Giessen, "Design principles for sensitivity optimization in plasmonic hydrogen sensors," ACS sensors **5**, 917 (2020).
18. S. Cai, A. Gonzalez-Vila, X. Zhang, T. Guo, and C. Caucheteur, "Palladium-coated plasmonic optical fiber gratings for hydrogen detection," Opt. Lett. **44**, 4483 (2019).
19. W. Chen, J. Niu, I. Liu, H. Chen, S. Cheng, K. Lin, and W. Liu, "Hydrogen sensing properties of a novel GaN/AlGaN Schottky diode decorated with palladium nanoparticles and a platinum thin film," Sens. Actuat. B Chem. **330**, 129339 (2021).
20. N. Strohfeldt, A. Tittl, and H. Giessen, "Long-term stability of capped and buffered palladium-nickel thin films and nanostructures for plasmonic hydrogen sensing applications," Opt. Mater. Express **3**, 194 (2013).
21. A. Tittl, P. Mai, R. Taubert, D. Dregely, N. Liu, and H. Giessen, "Palladium-based plasmonic perfect absorber in the visible wavelength range and its application to hydrogen sensing," Nano lett. **11**, 4366 (2011).
22. S. Chatterjee, E. Shkondin, O. Takayama, A. Fisher, A. Fraiwan, U. A. Gurkan, A. V. Lavrinenko, and G. Strangi, "Hydrogen gas sensing using aluminum doped ZnO metasurfaces," Nanoscale Adv. **2**, 3452 (2020).
23. T. Beni, N. Yamasaku, T. Kurotsu, N. To, S. Okazaki, T. Arakawa, A. Balcytis, G. Seniutinas, S. Juodkazis, and Y. Nishijima, "Metamaterial for hydrogen sensing," ACS sensors **4**, 2389 (2019).
24. S. Cai, F. Liu, R. Wang, Y. Xiao, K. Li, C. Caucheteur, and T. Guo, "Narrow bandwidth fiber-optic spectral combs for renewable hydrogen detection," Sci. China Inf. Sci. **63**, 222401 (2020).
25. Y. Nishijima, T. Kurotsu, N. Yamasaku, H. Takahashii, K. Kurihara, T. Beni, S. Okazaki, T. Arakawa, A. Balčytis, and G. Seniutinas, "Improvement and stabilization of optical hydrogen sensing ability of Au-Pd alloys," Opt. Express **28**, 25383 (2020).
26. Y. Nishijima, S. Shimizu, K. Kurihara, Y. Hashimoto, H. Takahashi, A. Balčytis, G. Seniutinas, S. Okazaki, J. Juodkazytė, T. Iwasa, T. Taketsugu, Y. Tominaga, and S. Juodkazis, "Optical readout of hydrogen storage in films of Au and Pd," Opt. Express **25**, 24081 (2017).
27. G. Zheng, H. Mühlenbernd, M. Kenney, G. Li, T. Zentgraf, and S. Zhang, "Metasurface holograms reaching 80% efficiency," Nat. Nanotechnol. **10**, 308 (2015).
28. T. Weiss, N. A. Gippius, S. G. Tikhodeev, G. Granet, and H. Giessen, "Derivation of plasmonic resonances in the Fourier modal method with adaptive spatial resolution and matched coordinates," J. Opt. Soc. Am. A **28**, 238 (2011).
29. https://refractiveindex.info.
30. M. Khanuja, B. R. Mehta, P. Agar, P. K. Kulriya, and D. K. Avasthi, "Hydrogen induced lattice expansion and crystallinity degradation in palladium nanoparticles: effect of hydrogen concentration, pressure, and temperature," J. Appl. Phys. **106**, 093515 (2009).
31. S. Syrenova, C. Wadell, F. A. Nugroho, T. A. Gschneidtner, Y. A. D. Fernandez, G. Nalin, D. Switlik, F. Westerlund, T. J. Antosiewicz, and V. P. Zhdanov, "Hydride formation thermodynamics and hysteresis in individual Pd nanocrystals with different size and shape," Nat. Mater. **14**, 1236 (2015).
32. R. Griessen, N. Strohfeldt, and H. Giessen, "Thermodynamics of the hybrid interaction of hydrogen with palladium nanoparticles," Nat. Mater. **15**, 311 (2016).
33. C. Bian, M. Li, W. Cao, M. Hu, Z. Chu, and R. Wang, "Robust integration of nitrogen-vacancy centers in nanodiamonds to optical fiber and its application in all-optical thermometry," Chin. Opt. Lett. **19**, 120601 (2021).